TITLE:

Spatial relationship between topography and rock uplift patterns in asymmetric mountain ranges based on a stream erosion model

AUTHOR(S):

Shikakura, Yosuke; Fukahata, Yukitoshi; Matsu'ura, Mitsuhiro

CITATION:

Shikakura, Yosuke ...[et al]. Spatial relationship between topography and rock uplift patterns in asymmetric mountain ranges based on a stream erosion model. Geomorphology 2012, 138(1): 162-170

ISSUE DATE:

2012-02

URL:

http://hdl.handle.net/2433/152387

RIGHT:

© 2011 Elsevier B.V.; この論文は出版社版でありません。引用の際には出版社版をご確認ご利用ください。; This is not the published version. Please cite only the published version.

京都大学学術情報リポジトリ
KURENAI 紅
Kyoto University Research Information Repository

京都大学 KYOTO UNIVERSITY
A Self-archived copy in
Kyoto University Research Information Repository
https://repository.kulib.kyoto-u.ac.jp
京都大学学術情報リポジトリ KURENAI 紅 Kyoto University Research Information Repository

Spatial relationship between topography and rock uplift patterns in asymmetric mountain ranges based on a stream erosion model

Yosuke Shikakura[a,*], Yukitoshi Fukahata[b], and Mitsuhiro Matsu'ura[c]

[a] *Department of Geophysics, Graduate School of Science, Kyoto University, Kitashirakawa Oiwake-cho, Sakyo-ku, Kyoto 606-8502, Japan*

[b] *Disaster Prevention Research Institute, Kyoto University, Gokasho, Uji, Kyoto 611-0011, Japan*

[c] *Institute of Statistical Mathematics, Tachikawa, Tokyo 190-8562, Japan*

*Corresponding Author: Yosuke Shikakura
Tel: +81 75 753-3948
Fax: +81 75 753-3714
E-mail: shikakura@kugi.kyoto-u.ac.jp

Yukitoshi Fukahata
E-mail: fukahata@rcep.dpri.kyoto-u.ac.jp

Mitsuhiro Matsu'ura
E-mail: mat-lab@ism.ac.jp

京都大学 KYOTO UNIVERSITY
A Self-archived copy in
Kyoto University Research Information Repository
https://repository.kulib.kyoto-u.ac.jp
京都大学学術情報リポジトリ KURENAI 紅 Kyoto University Research Information Repository

Abstract

The spatial relationship between topography and rock uplift patterns in asymmetric mountain ranges was investigated using a stream erosion model in which the asymmetric rock uplift was given and erosion rates were proportional to the m-th power of the drainage area and the n-th power of the channel gradient. The model conditions were simple, and thus the effects of horizontal rock movement, diffusional processes, and erosion thresholds were neglected, and spatially uniform precipitation, lithology, and vegetation were assumed. In asymmetric mountain ranges, under realistic exponent conditions ($m < n$) and the above assumptions, the surface erosion rate is faster on the steeper side and slower on the gentler side. The topographic axis migrates away from the rock uplift axis toward the center of the mountain range owing to the contrast in erosion rates. This migration continues until the erosion is balanced with rock uplift. In a dynamic steady state, the topographic pattern is independent of the rock uplift rate as indicated by an analytical solution, and is prescribed by the rock uplift pattern and the exponents m and n. As the asymmetry of the rock uplift pattern increases, the topographic axis migrates a greater distance. The location of the topographic axis is related to the location of the rock uplift axis by a simple logarithmic function, for a wide range of m and n. The fit of the numerical results and the logarithmic function is particularly good when $m = 0.5$ and $n = 1.0$. If the rock uplift pattern in asymmetric mountain ranges is known, the value of $n - 5m/4$ can be constrained based on the logarithmic relation, assuming a dynamic steady state. On the other hand, if the value of $n - 5m/4$ is known in an asymmetric mountain range, the rock uplift pattern can be estimated directly from the topography. This relation was applied to the Suzuka Range in central Japan, and the value of $n - 5m/4$ was estimated for an assumed reverse fault motion.

Keywords

rock uplift, topography, stream erosion model, asymmetric range, logarithmic relation

京都大学 KYOTO UNIVERSITY
A Self-archived copy in
Kyoto University Research Information Repository
https://repository.kulib.kyoto-u.ac.jp
京都大学学術情報リポジトリ KURENAI 紅 Kyoto University Research Information Repository

1. Introduction

Remarkable recent developments in geodetic techniques have produced detailed topographic information for the entire world (e.g., Farr et al., 2007). Detailed elevation maps have even been obtained for some satellites and planets, such as the moon (Araki et al., 2009) and Mars (Smith et al., 1999). In contrast, the data of tectonic movements are very limited in space and time. For example, even Japan's GEONET, one of the densest GPS networks in the world, provides crustal movement data at a spacing of about 20 km for a time span of less than two decades (Sagiya, 2004). Data relevant to the long-term tectonic movements (10^3–10^6 years or more) that control topographic evolution are even sparser. Information of long-term tectonic deformation is fundamentally important to deduce tectonic processes. A principal goal of tectonic geomorphology would be to extract information regarding the rates and patterns of tectonic deformation directly from topography.

The purpose of this study is to quantitatively estimate rock uplift rate patterns using the topography of asymmetric mountain ranges. Asymmetry of mountain ranges may be caused by horizontal rock movements (Adams, 1980; Willett et al., 2001; Herman and Braun, 2006; Miller et al., 2007), differential base levels of erosion (Ellis and Densmore, 2006), asymmetric distribution of rain and snow precipitation (Beaumont et al., 1992; Willett, 1999; Mitchell and Montgomery, 2006; Anders et al., 2008), or differences in lithology (Adams, 1980). Asymmetric rock uplift, however, should also result in asymmetric mountain ranges (Koons, 1989; Kooi and Beaumont, 1996; Kühni and Pfiffner, 2001). For example, the Suzuka Range in central Japan has been differentially uplifted by a west-dipping reverse fault system at the eastern margin of the range (Ota and Sangawa, 1984), which results in asymmetric topography.

In this study, asymmetric vertical rock uplift is considered to be a proxy for tectonic movement. Although lateral advection may be important in some asymmetric ranges, incorporating this effect requires the addition of more model parameters, such as the dip angle and length of the fault. Furthermore, natural faults commonly have some curvature. If even more realistic models are sought, for example, the elastic thickness of

京都大学 KYOTO UNIVERSITY
A Self-archived copy in
Kyoto University Research Information Repository
https://repository.kulib.kyoto-u.ac.jp
京都大学学術情報リポジトリ KURENAI 紅 Kyoto University Research Information Repository

the lithosphere must also be taken into account (e.g., Thatcher and Rundle, 1984; Fukahata and Matsu'ura, 2006). Although realistic, such complicated modeling is not the aim of this study, which focuses on a simpler set of conditions.

To express surface erosion, a stream erosion model (e.g., Howard and Kerby, 1983; Howard et al., 1994; Tucker and Slingerland, 1994) is used, in which the long-term erosion rate is proportional to the product of power functions for the drainage area and channel gradient. The values of the exponents of the power functions have been estimated in some mountain ranges from observed incision rates along river profiles (Stock and Montgomery, 1999; Whipple et al., 2000; van der Beek and Bishop, 2003; Harkins et al., 2007) and from the intrinsic concavity index of rivers with some assumptions of rock uplift rates under steady state conditions (e.g., Tarboton et al., 1989; Seidl and Dietrich, 1992; Kirby and Whipple, 2001; Meade, 2010). However, the relation between the values of the exponents and asymmetry of topography has not been elucidated.

The response of topography to asymmetric (gabled) vertical rock uplift is examined using the stream erosion model. The location of main drainage divides (topographic axes) is of particular importance because these divides determine the first-order topographic features and drainage patterns in mountain ranges, which prescribe the environment and landscape of the area. If there is no erosion, the topographic axis must simply coincide with the rock uplift axis. Under asymmetric rock uplift and fluvial erosion, however, the erosion rate is seemingly faster on the steeper side, as long as all other conditions that contribute to erosion rate, such as precipitation, lithology, and vegetation, are uniform. Asymmetric uplift and stream erosion would predict, therefore, that the topographic axis migrates away from the rock uplift axis toward the center of the mountain range. The aim of this study is to systematically quantify the distance between the topographic and rock uplift axes. Because the distance also depends on the exponent values of the stream erosion model, this study links to estimation of these values.

This study employs a topographic evolution model that incorporates the effect of

京都大学 KYOTO UNIVERSITY
A Self-archived copy in
Kyoto University Research Information Repository
https://repository.kulib.kyoto-u.ac.jp
京都大学学術情報リポジトリ KURENAI 紅 Kyoto University Research Information Repository

109 rock uplift into a stream erosion model. Under conditions of asymmetric rock uplift,
110 topographic evolution is numerically simulated, and a curious relationship between
111 topographic and rock uplift axes is shown. We then investigate the dependence of the
112 relation on the values of the exponents, and discuss the implications of the results for
113 real mountain ranges.
114
115 **2. Topographic evolution model**
116 The stream erosion model is suitable for modeling fluvial erosion at a resolution of
117 1 km and was developed based on the law of open channel flow for stream incision
118 into bedrock (e.g., Howard and Kerby, 1983; Howard et al., 1994; Tucker and
119 Slingerland, 1994). In the stream erosion model, the erosion rate ε is expressed as
120 the product of power functions for the drainage area A and channel gradient S as
121 follows:
122
123 $$\varepsilon(x,y,t) = K\left[A(x,y,t)\right]^m \left[S(x,y,t)\right]^n \quad (1)$$
124
125 where K is the coefficient of erosion and the dimensionless exponents m and n are
126 positive constants related to basin hydrology, hydraulic geometry, and erosion process
127 (Howard et al., 1994; Whipple and Tucker, 1999; Whipple et al., 2000). In the present
128 study, surface deposition (e.g., Willgoose et al., 1991; Kooi and Beaumont, 1994;
129 Tucker and Whipple, 2002), and hillslope processes (e.g., Schmidt and Montgomery,
130 1995; Roering et al., 1999; Stark and Hovius, 2001; Anderson, 2002) were neglected,
131 and the erosion threshold that depends on the critical shear stress (e.g., Howard et al.,
132 1994; Whipple and Tucker, 1999; Tucker and Bras, 2000; Lague et al., 2005) was not
133 employed, for simplicity. Other factors that contribute to erosion rate, such as
134 precipitation, lithology, and vegetation, are assumed to be spatially and temporally
135 uniform.
136 Rock uplift u is incorporated into the stream erosion model of Eq. (1) as in many

京都大学 KYOTO UNIVERSITY
A Self-archived copy in
Kyoto University Research Information Repository
https://repository.kulib.kyoto-u.ac.jp
京都大学学術情報リポジトリ KURENAI 紅 Kyoto University Research Information Repository

137 previous studies (e.g., Willgoose et al., 1991; Kirkby, 1994; Tucker and Slingerland,
138 1994; Kirby and Whipple, 2001; Miller et al., 2007) as
139
140 $$\frac{d}{dt}h(x,y,t) = u(x,y,t) - K\left[A(x,y,t)\right]^m \left[S(x,y,t)\right]^n \quad (2)$$
141
142 where h represents altitude. The drainage area A and the channel gradient S are
143 functions of h. In other words, if a topographic distribution $h(x,y,t)$ is given,
144 $A(x,y,t)$ and $S(x,y,t)$ are uniquely determined. Parameter S is the gradient of h. A
145 is dependent on h in a complex fashion, but a proportional change in h from $h(x,y)$
146 to $ch(x,y)$, where c is an arbitrary positive constant, does not affect A.
147 Given the rock uplift rate $u(x,y,t)$, the initial height $h(x,y,0)$, and the boundary
148 conditions, Eq. (2) can be solved with a finite difference method. Following the
149 scheme developed by Beaumont et al. (1992), the model can be discretized in space
150 and time. A series of regular square poles is used to represent the discretized
151 topography. The drainage area and channel gradient for each cell is computed using a
152 steepest-descent flow accumulation algorithm (Tucker and Slingerland, 1994). In
153 computing the drainage area for a particular cell, the area of that cell is included. If the
154 cell concerned is not included, the drainage divide is fixed and can not migrate because
155 the erosion rate at the headwater cell of each stream is always zero as there is zero
156 drainage area.
157 In the numerical simulation, the model area is 100×100 km, which is divided into
158 1×1 km cells. The x-axis is the east direction, and the y-axis is the north direction. The
159 origin $(x,y) = (0,0)$ is at the center of the model area.
160 The asymmetric rock uplift rate in the x direction is given by the following
161 function:
162

京都大学 KYOTO UNIVERSITY
A Self-archived copy in
Kyoto University Research Information Repository
https://repository.kulib.kyoto-u.ac.jp
京都大学学術情報リポジトリ KURENAI 紅 Kyoto University Research Information Repository

$$u(x,y,t)=\begin{cases}\dfrac{x+L}{x_u+L}u_{max} & (-L\le x\le x_u)\\ \dfrac{L-x}{L-x_u}u_{max} & (x_u\le x\le L)\end{cases} \quad (3)$$

where L is half of the model length (L= 50 km). The functional form is shown in Fig. 1. x_u represents the location of the rock uplift axis, and u_{max} represents the maximum rock uplift rate, which is equal to the rock uplift rate at the rock uplift axis x_u. The rock uplift rate is uniform in the y direction and constant over time.

[Insert Fig. 1]

The initial conditions are a flat topography at an elevation of 0 m, with white noise with maximum amplitude of 10 m. The altitudes of the eastern and western boundaries are exactly set at 0 m through the computation. The water drains only through the eastern and western boundaries, and the northern and southern sides are no-flow boundaries. The problems associated with closed depressions (e.g., Tucker et al., 2001) are not included because the gradient of slopes generated by the following computations is usually very steep, except for just after initiation of rock uplift. For closed depressions, the erosion rate is set to zero.

3. Results

The relationship between rock uplift and topography was quantitatively investigated with the topographic evolution model introduced above. Different values for parameters x_u and u_{max}, which prescribe the rock uplift rate, were used in order to determine the dependence of topography on these parameters. In contrast, parameters m, n, and K, which control the erosion rate, were initially fixed at m = 0.5, n = 1.0, and $K=1.2\times10^{-5}$ yr^{-1}. These values imply that the stream incision rate was modeled as a function of stream power per unit bed area (e.g., Whipple and Tucker,

京都大学 KYOTO UNIVERSITY
A Self-archived copy in
Kyoto University Research Information Repository
https://repository.kulib.kyoto-u.ac.jp
京都大学学術情報リポジトリ KURENAI 紅 Kyoto University Research Information Repository

189 1999). As discussed in Section 3.4, the dependence of topography on these parameters
190 was also examined.
191
192 **3.1 Topographic evolution under asymmetric rock uplift**
193 The rock uplift parameters x_u and u_{max} were initially set at 30 km and 6 mm yr^{-1},
194 respectively, to observe the topographic evolution process (Fig. 2). The results show
195 that after initiation of rock uplift, the mountain grows at approximately the same rate as
196 uplift because erosion is very weak. The topographic axis, defined here as the line of the
197 highest mean altitude along the north-south profiles, coincides almost exactly with the
198 rock uplift axis. However, as the mountain grows, surface erosion increases, especially
199 on the side of the range having the steepest topographic gradient (east). The topographic
200 axis thus gradually migrates toward the center of the mountain range (Fig. 2). This
201 means that the location of the topographic axis is more strongly affected by the effect of
202 the channel gradient S than by the drainage area A, which is larger on the less steep side.
203 A dynamic steady state is reached before t = 4.0 My. A dynamic steady state is defined
204 as the condition under which the elevation change over a 1 My interval, averaged over
205 the model area and normalized by the maximum elevation, is less than 0.01%. Before
206 reaching a steady state, the topographic axis migrates about 10 km from the rock uplift
207 axis toward the center. The elevation of the topographic axis is slightly reduced during
208 this migration.
209
210 [Insert Fig. 2]
211
212 **3.2 Relationship between rock uplift and topography**
213 The relation of asymmetric rock uplift to topographic evolution was simulated by
214 changing the maximum uplift rate u_{max} and the location of the rock uplift axis x_u.
215 Values of 2, 6, and 10 mm yr^{-1} were used for u_{max}, and x_u was taken every 5 km
216 from 5 to 45 km for each u_{max}. To suppress the dependence of topographic evolution
217 on the initial random noise, the numerical simulation was performed five times for

京都大学 KYOTO UNIVERSITY
A Self-archived copy in
Kyoto University Research Information Repository
https://repository.kulib.kyoto-u.ac.jp
京都大学学術情報リポジトリ KURENAI 紅 Kyoto University Research Information Repository

each u_{max} and x_u pair by changing the random noise of the initial topography. Fig. 3 shows the relation between u_{max} and the location of the topographic axis in the steady state x_t for various values of x_u. As shown in the figure, x_t does not depend on u_{max} irrespective of x_u. In the simulation of topographic evolution based on Eq. (2), the pattern of topography in the steady state is generally independent of the rate of rock uplift for the following reason. In the steady state, the left side of Eq. (2) is zero:

$$u(x,y) = K[A(x,y)]^m[S(x,y)]^n \tag{4}$$

Therefore, if a topographic distribution $h(x,y)$ is a solution of Eq. (4) under a given uplift rate $u(x,y)$, $\sqrt[n]{c}h(x,y)$ is also a solution for another given uplift rate with the same pattern $cu(x,y)$, where c is an arbitrary positive constant. Recall that a proportional change in height distribution from $h(x,y)$ to $c'h(x,y)$ does not affect the drainage area $A(x,y)$; only the channel gradient changes from $S(x,y)$ to $c'S(x,y)$. The minor fluctuation of each line in Fig. 3 is ascribed to the given random noise added to the initial topography. In brief, a proportional change in u from $u(x,y)$ to $cu(x,y)$ results in no change in A and a proportional change in S from $S(x,y)$ to $\sqrt[n]{c}S(x,y)$ in the steady state. Here, it should be noted that u, K and m may be spatially variable, but n must be constant in space.

[Insert Fig. 3]

From the theoretical relations described above, the height of the topographic axis in the steady state should be proportional to the rock uplift rate to the $1/n$ power. Given that n is taken to be unity, we show the elevation of the topographic axis in the steady state h_{max} normalized by u_{max} as a function of x_u in Fig. 4A. Each line of different rock uplift rates overlaps almost completely with each other. This means that h_{max} is indeed proportional to rock uplift rate. In addition, h_{max} decreases with x_u, which is consistent with the topographic evolution process shown in Fig. 2, where the elevation

京都大学 KYOTO UNIVERSITY
A Self-archived copy in
Kyoto University Research Information Repository
https://repository.kulib.kyoto-u.ac.jp
京都大学学術情報リポジトリ KURENAI 紅 Kyoto University Research Information Repository

247 of the topographic axis decreases as the topographic axis moves away from the rock
248 uplift axis x_u toward the center. The distance between x_u and x_t increases with
249 x_u, as shown in Fig. 3 and Fig. 5.
250
251 [Insert Fig. 4]
252
253 Fig. 4B shows the time required to reach a dynamic steady state for each x_u and
254 u_{max} pair. As expected, the time to reach a steady state is longer for larger x_u. The
255 topographic axis slowly moves from the rock uplift axis toward the center of the
256 mountain range (Fig. 2), and the distance increases with x_u (Fig. 3). During this time,
257 the drainage network continues to evolve and adapt. This process takes time.
258 Comparison of Fig. 4A and B shows that the time required is most sensitive to the
259 initial random noise.
260 The time required is also independent of the maximum rock uplift rate u_{max} (Fig.
261 4B). For this independence, the key is that n is taken to be unity. When a height
262 distribution $h(x,y,t)$ is a solution of Eq. (2) for a given uplift rate $u(x,y,t)$ that is
263 constant in time, the height distribution $ch(x,y,t)$ is also a solution for another given
264 uplift rate with the same pattern $cu(x,y,t)$. Recall again the drainage area $A(x,y,t)$ is
265 constant for a proportional change in height distribution from $h(x,y,t)$ to $ch(x,y,t)$
266 and that $S(x,y,t)$, which is the gradient of $h(x,y,t)$, is proportional to $h(x,y,t)$. In
267 brief, the proportional relation of topography to rock uplift rates holds true throughout
268 the time development. However, it should be noted that the proportional relation does
269 not hold true when $n \neq 1$; only in the steady state, the proportional relation of
270 topography to the n-th root of the rock uplift rate (Fig. 3 and Fig. 4A) holds true for
271 $n \neq 1$. The independence of the elapsed time relative to the magnitude of rock uplift rate
272 has already been noted by Kooi and Beaumont (1996) for the case of symmetric rock
273 uplift. The independence is also valid for asymmetric rock uplift.
274
275 **3.3 Logarithmic relation between topographic and rock uplift axes**

京都大学 KYOTO UNIVERSITY
A Self-archived copy in
Kyoto University Research Information Repository
https://repository.kulib.kyoto-u.ac.jp
京都大学学術情報リポジトリ KURENAI 紅 Kyoto University Research Information Repository

The relation between the rock uplift axis x_u and the topographic axis x_t in the steady state (Fig. 3) requires examination. Any proportional change in a given rock uplift rate, from $u(x,y)$ to $cu(x,y)$, does not affect the location of the topographic axis under steady-state conditions (and for transient behavior when $n=1$). The numerical simulation was run five times for each u_{max} and x_u pair, and the average and standard deviation of 15 trials with different rock uplift rates were assessed as a group.

The results show that x_t increases with x_u (Fig. 5), but the rate of increase in x_t is not as rapid as that in x_u. The numerical relation between x_t and x_u needs to be expressed with an analytical function. The function must increase monotonically and the differentiation of the function should decrease monotonically; therefore, a logarithmic function would be appropriate. As a boundary condition, the function must pass through the origin $(x_u = x_t = 0)$ because there is no need for the topographic axis to move away from the center of the model region when x_u equals zero. In addition, a very small change in x_u from zero seems to cause the same amount of change in x_t. This condition is written as $dx_t / dx_u = 1$ at $x_u = 0$. The logarithmic function to fit the numerical relation is then expressed by

$$x_t = f(x_u) = a \ln\left(\frac{x_u}{a} + 1\right) \tag{5}$$

A natural logarithmic function is used here, but even if an apparently different base is used for the logarithmic function, the functional form is the same as Eq. (5) after transformation of the base. Eq. (5) consists of only the fitting parameter *a*, which is determined using the least-square method.

[Insert Fig. 5]

The fit of the logarithmic function to the numerical results is statistically significant

京都大学 KYOTO UNIVERSITY
A Self-archived copy in
Kyoto University Research Information Repository
https://repository.kulib.kyoto-u.ac.jp
京都大学学術情報リポジトリ KURENAI 紅 Kyoto University Research Information Repository

(Fig. 5). The function passes almost exactly through the average of each trial. The average misfit to the nine data points is less than 0.2 km, which is much smaller than the grid interval of the numerical simulation. It should be noted that the result of each trial does not necessarily fit the logarithmic function, as shown by the error bar representing the standard deviation. After many trials with different initial random noise, however, the averages of the results follow the natural logarithmic function.

So far, parameters m, n, and K, which control erosion rates, have been fixed. Parameter K does not affect the functional relation between x_t and x_u because K has the same effect (except for the reciprocal) as u (Eq. (4)). However, x_t does depend on m and n. The effect of the exponents m and n on the logarithmic relation between x_t and x_u requires investigation.

3.4 Dependence of the logarithmic relation on the exponents

As explained by Tucker and Whipple (2002), Eq. (1) has been used to model various fluvial erosion processes, including bed shear stress ($m \simeq 0.3, n \simeq 0.7$) (Howard and Kerby, 1983; Howard et al., 1994; Tucker and Slingerland, 1997), stream power per unit channel length ($m \simeq n = 1.0$) (Seidl and Dietrich, 1992), and stream power per unit bed area ($m \simeq 0.5, n \simeq 1.0$) (Stock and Montgomery, 1999; Whipple and Tucker, 1999; Kirby and Whipple, 2001). They also pointed out that the computed stream profile concavity under the condition $m/n \geq 1.0$ or $m/n < 0.2$ is not common for most mountain drainage basins.

The values of the exponents m and n as well as those of x_u and u_{max} are changed: n is set at 0.5, 1.0, and 1.5, and m/n has values that increase in increments of 0.1, from 0.3 to 0.8, for each value of n. For each pair of m and n, the same computation as in Fig. 5 is repeated, and the relationship between the location of the topographic axis in the steady state x_t and that of the rock uplift axis x_u for each pair of exponents m and n is plotted (Fig. 6). The fit of the logarithmic function is again very good for most cases, indicating that the value of the fitting parameter a can be determined from one datum point of x_t and x_u, regardless of the values of the

京都大学 KYOTO UNIVERSITY
A Self-archived copy in
Kyoto University Research Information Repository
https://repository.kulib.kyoto-u.ac.jp
京都大学学術情報リポジトリ KURENAI 紅 Kyoto University Research Information Repository

exponents *m* and *n*. The fit appears to be best when $m/n = 0.5$. For smaller m/n, the numerical results appear to be slightly more rectilinear than the logarithmic function, as for example in the case of $m/n = 0.3$. For larger m/n, the fit is still good. This may be due to the characteristics of the fitting function. The fitting function asymptotically approaches $x_t = x_u$ as m/n increases (Fig. 6). Therefore, even if the theoretical fitting function deviated from the logarithmic function, the deviation would not be noticeable.

[Insert Fig. 6]

The change in the fitting function in Fig. 6 corresponds to the change in the fitting parameter *a* in Eq. (5). For larger *a*, the fitting function approaches $x_t = x_u$, but for smaller *a*, the curvature of the fitting function becomes more acute. The value of *a* is controlled by the relative susceptibility of drainage area *A* and channel gradient *S* to erosion. The relative contribution of the drainage area, which is larger on the gentler side, increases with larger m/n. This means that for larger m/n, the topographic axis x_t does not move away from the rock uplift axis x_u as much, the fitting function approaches $x_t = x_u$, and *a* becomes large. In contrast, for smaller m/n, the topographic axis migrates a substantial distance, the curvature of the fitting function is more acute, and the fitting parameter *a* becomes smaller. As shown in Fig. 6, however, the value of *a* can vary significantly for smaller m/n, even if m/n has the same value. In short, parameter *a* is not dependent only on m/n.

A contour map of parameter *a* on the *m* and *n* coordinate plane (Fig. 7A) shows that *a* is roughly constant for $n - pm$, where *p* is about 5/4. If *a* is then plotted relative to $n - pm + q$ on a double logarithmic diagram (Fig. 7B) where *q* is a constant parameter, the numerical results can be fitted by a linear function expressed as

$$\log_{10} a = r \log_{10}(n - pm + q) + s \quad (6)$$

京都大学 KYOTO UNIVERSITY
A Self-archived copy in
Kyoto University Research Information Repository
https://repository.kulib.kyoto-u.ac.jp
京都大学学術情報リポジトリ KURENAI 紅 Kyoto University Research Information Repository

where the optimal parameter values determined with the least-square method are $p = 1.26$, $q = 0.415$, $r = -2.55$, and $s = 1.11$. The fit is again excellent. If $p = 1.25$ is used instead of $p = 1.26$, the fit is nearly the same. This means that $n - 5m/4$ is an appropriate indicator of the relative susceptibility of drainage area A and channel gradient S to erosion. For smaller $n - 5m/4$, in which the contribution of the drainage area is relatively high, the value of a becomes larger, and vice versa. With Eqs. (5) and (6), the relation between x_t and $n - 5m/4$ are obtained for various values of x_u (Fig. 8). This diagram means that we can estimate $n - 5m/4$ or x_u, if we know either value of them, because the topography (i.e., x_t) is commonly well known.

[Insert Fig. 7], [Insert Fig. 8]

4. Discussion

As shown in the numerical simulations, the erosion rate in asymmetric mountain ranges is faster on the steeper side and slower on the gentler side under realistic exponent conditions ($m < n$), as long as the other conditions that contribute to erosion rate are uniform. For example, in the Taiwan Central Range, where the eastern slope is much steeper than the western slope, significantly faster erosion is suggested for the eastern flank as compared to the western flank, as indicated by the metamorphic grades of exposed rocks (Ho, 1986), fission track analyses (Willett et al., 2003), and heat-flow data (Yamano, 1995; Fukahata and Matsu'ura, 2001).

To address the distance migrated by the topographic axis relative to the rock uplift axis, the model was applied to the Suzuka Range in central Japan as an example (Fig. 9A). The Suzuka Range is located in the Kinki Triangle (Huzita, 1962), an area currently under east-west compression (Huzita, 1980; Terakawa and Matsu'ura, 2010). The eastern limit of the Suzuka Range is bounded by west-dipping reverse faults of the Ichishi Fault system, which have been active since the late Pliocene (Ota and Sangawa, 1984; Ishiyama et al., 1999). There is no significant local variation in lithology (Huzita, 1962; Geological Survey of Japan, AIST, 2009) and precipitation across the range.

京都大学 KYOTO UNIVERSITY
A Self-archived copy in
Kyoto University Research Information Repository
https://repository.kulib.kyoto-u.ac.jp
京都大学学術情報リポジトリ KURENAI 紅 Kyoto University Research Information Repository

391

392 [Insert Fig. 9]

393

394 A cross-section of the topographic profile of the range (Fig. 9B) was produced by
395 averaging the elevation data in the direction parallel to the trend of the range
396 (approximately north-south, Fig. 9A). In the topographic profile, the horizontal
397 distance and relative elevation of the mountain range are normalized by the width of
398 the range L_R (20 km) and the difference between the maximum (812 m) and
399 minimum (170 m) heights. The topographic axis of the Suzuka Range is located at
400 about 0.20 (normalized distance) as shown in Fig. 9B.

401 The uplift and erosion rates across the Suzuka Range are not known. A seismic
402 reflection survey showed that the Fumotomura Fault, one of the faults of the Ichishi
403 Fault system, has a dip angle of about 60˚ at shallow depth (Ishiyama et al., 1999). The
404 youngest strata, the Tokai Group, are cross-cut by the fault, but the displacement is
405 very small. West of the fault, strata of the Tokai Group steeply dip eastward, indicating
406 that deformation around the eastern end of the range is caused by a fault-propagation
407 fold (Ishiyama et al., 1999). Based on the seismic survey, we simulated the crustal
408 deformation pattern in the Suzuka Range. The fault was assumed to have a dip angle of
409 60˚ at the earth's surface, which gradually changes to a horizontal detachment fault at
410 depth (Fig. 10A). The slip rate along the fault was assumed to decrease gradually to
411 zero at surface from 3 km at depth because the deformation is caused by a
412 fault-propagation fold. It should be noted that the true fault geometry and slip rate
413 distribution are not well determined from observations; the configuration described
414 was adopted to demonstrate the use of the model described in the previous section. In
415 the computation of crustal deformation due to the dislocation across the fault plane, an
416 elastic half-space was assumed and a value of 50 GPa was used for the bulk modulus
417 and 30 GPa for the shear modulus.

418

419 [Insert Fig. 10]

京都大学 KYOTO UNIVERSITY
A Self-archived copy in
Kyoto University Research Information Repository
https://repository.kulib.kyoto-u.ac.jp
京都大学学術情報リポジトリ KURENAI 紅 Kyoto University Research Information Repository

Fig. 10B and C shows the profiles of vertical and horizontal displacements, respectively. The rock uplift axis is located at 0.32 in normalized distance (Fig. 10B). When $x_u = 0.32$ and $x_t = 0.20$, we can obtain the estimate of $n - 5m/4$ to be 0.38 ± 0.05 based on Fig. 8, where the estimation error is originated from the standard deviation shown in Fig. 6. $n - 5m/4 = 0.38$ almost coincides with a typically used set of the exponent values of $(m,n) = (0.5,1.0)$. Then, $n - 5m/4$ is 0.375. If the topography of the Suzuka Range is before the dynamic steady state, the value of $n - 5m/4$ becomes larger, because x_t further moves toward the center of the range.

So far, only the purely gabled rock uplift pattern has been considered as a cause of topographic asymmetry. In actual mountain ranges, however, the other factors may significantly affect the relation between the rock uplift axis x_u and the topographic axis x_t. So, we carried out some sensitivity tests, in which $x_u = 0.32$ and $(m,n) = (0.5,1.0)$ were used, and the topographic evolution was computed 15 times for each setting with different initial random noise.

As shown in Fig. 10B and C, the computed uplift pattern is not purely gabled and the horizontal displacement is not zero. Thus, the computed displacement profiles (solid lines in Fig. 10B and C) were used in the numerical simulation of topographic evolution, instead of the purely gabled rock uplift pattern (dotted line in Fig. 10B). As a result, 0.217 ± 0.007 was obtained for x_t. This value is close to 0.207 ± 0.010, which is obtained for the purely gabled rock uplift pattern. If the horizontal displacement is neglected and only the computed uplift profile (solid line in Fig. 10B) is used, 0.225 ± 0.012 is obtained. The effect of horizontal displacement is not significant in this situation, because the horizontal displacement in the hanging wall is quite uniform (Fig. 10C). The effect of asymmetrical precipitation was also investigated by giving 20 % larger precipitation (larger A in the simulation) in one side. The topographic axis at each time step was used as the boundary of the different precipitation. Then, x_t is 0.179 ± 0.011 and 0.227 ± 0.007 for larger precipitation in the eastern and western sides, respectively. When the base level of erosion was changed 10 % in the normalized

京都大学 KYOTO UNIVERSITY
A Self-archived copy in
Kyoto University Research Information Repository
https://repository.kulib.kyoto-u.ac.jp
京都大学学術情報リポジトリ KURENAI 紅 Kyoto University Research Information Repository

449 height, x_t was 0.189 ± 0.014 and 0.223 ± 0.010 for the higher base level in the
450 western and eastern sides, respectively. In either case, the calculated x_t is almost
451 within the two sigma of the purely gabled uplift case demonstrated in the previous
452 section.

453 In the numerical simulation, the effects of thresholds for erosion and hillslope
454 processes were omitted for simplicity. Owing to this simplification, the numerical
455 model is essentially described by only three parameters, the rock uplift axis x_u and
456 the exponents *m* and *n*, and does not depend on the rock uplift rate (Fig. 3 and Fig. 4)
457 or the coefficient of erosion *K*. Numerical experiments in which a threshold of critical
458 shear stress for stream erosion is included do not cause notable changes, probably due
459 to a rapid erosion rate in the numerical simulation. Although the model does not
460 explicitly incorporate hillslope processes, the uppermost cells of streams can be eroded
461 because the area of any given cell is included in the calculation of the drainage area.
462 This differs from the models of Kooi and Beaumont (1996) and Kühni and Pfiffner
463 (2001). If we incorporate hillslope processes into the model, the migration distance of
464 the topographic axis would probably be larger because the second derivative of the
465 topography $\nabla^2 h$ would be reduced. The main features of the topography, however,
466 are considered to be primarily controlled by an advective stream process (Howard,
467 1994; Kooi and Beaumont, 1996). In fact, the numerical simulation of Miller et al.
468 (2007), in which the scale of their target (Siwalik Hills, Nepal) is about 20 km in the
469 horizontal direction, demonstrated that diffusion does not visibly affect the asymmetry
470 of the range under normal conditions.

471 This study identifies the logarithmic relation between the topographic and rock
472 uplift axes for a simple set of conditions (Fig. 5 and Fig. 6). The fitting parameter *a* of
473 the logarithmic function was also clearly related to the exponents *m* and *n* (Fig. 7). To
474 reveal the nature of the logarithmic relation, we tried to derive these relations
475 analytically, but failed despite of its simplicity. This problem should be addressed in
476 the future.
477

京都大学 KYOTO UNIVERSITY
A Self-archived copy in
Kyoto University Research Information Repository
https://repository.kulib.kyoto-u.ac.jp
京都大学学術情報リポジトリ KURENAI 紅 Kyoto University Research Information Repository

5. Conclusions

Asymmetric rock uplift is one of the main causes of asymmetric mountain ranges, such as the Suzuka Range in central Japan. In asymmetric mountain ranges, the surface erosion rate is faster on the steeper side and slower on the gentler side, under realistic conditions for the exponents ($m < n$) and assuming that the other conditions that control the erosion rate, such as precipitation, lithology, and vegetation, are uniform. Therefore, the topographic axis migrates from the rock uplift axis toward the center of the mountain range until erosion is balanced by rock uplift (Fig. 2); this balancing takes a few million years (Fig. 4).

The migration distance from the rock uplift axis can be expressed by a logarithmic function (Fig. 6). The fit of the logarithmic function is especially good when $(m, n) = (0.5, 1.0)$ (Fig. 5). A proportional change in the uplift rate does not affect this relationship (Fig. 3 and Fig. 4) because a change in the uplift rate from $u(x, y)$ to $cu(x, y)$ results in no change in the drainage area A and a proportional change in S from $S(x, y)$ to $\sqrt[n]{c}S(x, y)$. Here, u, K, and m may be spatially variable, but n must be constant.

If the rock uplift pattern for an asymmetric mountain range is similar to be gabled, the value of $n - 5m/4$ can be constrained (Fig. 8). This concept was applied to the Suzuka Range in central Japan (Fig. 9 and Fig. 10). Conversely, if a value of $n - 5m/4$ is available, the rock uplift pattern can be estimated directly from the topography in asymmetric mountain ranges.

Acknowledgements

We thank Tatsuya Ishiyama for his useful comments. We also acknowledge the comments by Takashi Oguchi and anonymous reviewers in improving the manuscript. Figures were plotted using the GMT software (Wessel and Smith, 1998).

京都大学 KYOTO UNIVERSITY
A Self-archived copy in
Kyoto University Research Information Repository
https://repository.kulib.kyoto-u.ac.jp
京都大学学術情報リポジトリ KURENAI 紅 Kyoto University Research Information Repository

505 **References**

506

507 Adams, J., 1980. Contemporary uplift and erosion of the Southern Alps, New Zealand.
508 Geological Society of America Bulletin 91, 1–114.
509 Anders, A.M., Roe, G.H., Montgomery, D.R., Hallet, B., 2008. Influence of
510 precipitation phase on the form of mountain ranges. Geology 36, 479–482.
511 Anderson, R.S., 2002. Modeling the tor-dotted crests, bedrock edges, and parabolic
512 profiles of high alpine surfaces of the Wind River Range, Wyoming.
513 Geomorphology 46, 35–58.
514 Araki, H., Tazawa, S., Noda, H., Ishihara, Y., Goossens, S., Sasaki, S., Kawano, N.,
515 Kamiya, I., Otake, H., Oberst, J., Shum, C., 2009. Lunar Global Shape and Polar
516 Topography Derived from Kaguya-LALT Laser Altimetry. Science 323, 897–900.
517 Beaumont, C., Fullsack, P., Hamilton, J., 1992. Erosional control of active
518 compressional orogens. In: McClay, K.R. (Ed.), Thrust Tectonics. Chapman and
519 Hall, London. pp. 1–18.
520 Ellis, M.A., Densmore, A.L., 2006. First-order topography over blind thrusts. In:
521 Willett, S.D., Hovius, N., Brandon M.T., Fisher, D. (Eds.), Tectonics, Climate, and
522 Landscape Evolution. Geological Society of America Bulletin Special Paper 398, pp.
523 251–266.
524 Farr, T.G., Rosen, P.A., Caro, E., Crippen, R., Duren, R., Hensley, S., Kobrick, M.,
525 Paller, M., Rodriguez, E., Roth, L., Seal, D., Shaffer, S., Shimada, J., Umland, J.,
526 Werner, M., Oskin, M., Burbank, D., Alsdorf, D., 2007. The Shuttle Radar
527 Topography Mission. Reviews of Geophysics 45, RG2004,
528 doi:10.1029/2005RG000183.
529 Fukahata, Y., Matsu'ura, M., 2001. Correlation between surface heat flow and elevation
530 and its geophysical implication. Geophysical Research Letters 28, 2703–2706.
531 Fukahata, Y., Matsu'ura, M., 2006. Quasi-static internal deformation due to a
532 dislocation source in a multilayered elastic/viscoelastic half-space and an
533 equivalence theorem. Geophysical Journal International 166, 418–434.

京都大学 KYOTO UNIVERSITY
A Self-archived copy in
Kyoto University Research Information Repository
https://repository.kulib.kyoto-u.ac.jp
京都大学学術情報リポジトリ KURENAI 紅 Kyoto University Research Information Repository

534 Geographical Survey Institute of Japan, 1997. Digital map 50 m grid (Elevation)
535 Nippon III (CD-ROM).
536 Geological Survey of Japan, AIST, 2009. Seamless digital geological map of Japan 1:
537 200,000, Dec 15, 2009 version, Research Information Database DB084, Geological
538 Survey of Japan, National Institute of Advanced Industrial Science and Technology.
539 Harkins, N., Kirby, E., Heimsath, A., Robinson, R., Reiser, U., 2007. Transient fluvial
540 incision in the headwaters of the Yellow River, northeastern Tibet, China. Journal of
541 Geophysical Research 112, F03S04, doi:10.1029/2006JF000570.
542 Herman, F., Braun, J., 2006. Fluvial response to horizontal shortening and glaciations:
543 A study in the Southern Alps of New Zealand. Journal of Geophysical Research 111,
544 F01008, doi:10.1029/2004JF000248.
545 Ho, C.S., 1986. A synthesis of the geologic evolution of Taiwan. Tectonophysics 125,
546 1–16.
547 Howard, A.D., 1994. A detachment-limited model of drainage basin evolution. Water
548 Resources Research 30, 2261–2285.
549 Howard, A.D., Kerby, G., 1983. Channel changes in badlands. Geological Society of
550 America Bulletin 94, 739–752.
551 Howard, A.D., Dietrich, W.E., Seidl, M.A., 1994. Modeling fluvial erosion on regional
552 to continental scales. Journal of Geophysical Research 99, 13971–13986.
553 Huzita, K., 1962. Tectonic development of the Median Zone (Setouchi) of Southwest
554 Japan since the Miocene, with special reference to the characteristic structure of
555 Central Kinki Area. Journal of Geoscience, Osaka City University 6, 103–144.
556 Huzita, K., 1980. Role of the Median Tectonic Line in the Quaternary tectonics of
557 Japanese Islands. Memoirs of the Geological Society of Japan 18, 129–153.
558 Ishiyama, T., Takemura, K., Okada A., 1999. Structural growth rate of the eastern
559 margin of the Suzuka Range during Quaternary. Journal of the Seismological
560 Society of Japan 52, 229–240 (in Japanese with English abstract).
561 Kirby, E., Whipple, K., 2001. Quantifying differential rock-uplift rates via stream
562 profile analysis. Geology 29, 415–418.

京都大学 KYOTO UNIVERSITY
A Self-archived copy in
Kyoto University Research Information Repository
https://repository.kulib.kyoto-u.ac.jp
京都大学学術情報リポジトリ KURENAI 紅 Kyoto University Research Information Repository

563 Kirkby, M.J., 1994. Thresholds and instability in stream head hollows: A model of
564 magnitude and frequency for wash processes. In: Kirkby, M.J. (Ed.), Process Models
565 and Theoretical Geomorphology. Wiley, Chichester, pp. 295–314.
566 Kooi, H., Beaumont, C., 1994. Escarpment evolution on high-elevation rifted margins:
567 Insights derived from a surface processes model that combines diffusion, advection,
568 and reaction. Journal of Geophysical Research 99, 12191–12209.
569 Kooi, H., Beaumont, C., 1996. Large-scale geomorphology: Classical concepts
570 reconciled and integrated with contemporary ideas via a surface processes model.
571 Journal of Geophysical Research 101, 3361–3386.
572 Koons, P.O., 1989. The topographic evolution of collisional mountain belts: A
573 numerical look at the Southern Alps, New Zealand. American Journal of Science
574 289, 1041–1069.
575 Kühni, A., Pfiffner, O.A., 2001. Drainage patterns and tectonic forcing: a model study
576 for the Swiss Alps. Basin Research 13, 169–197.
577 Lague D., Hovius N., Davy P., 2005. Discharge, discharge variability, and the bedrock
578 channel profile. Journal of Geophysical Research 110, F04006,
579 doi:10.1029/2004JF000259.
580 Meade, B.J., 2010. The signature of an unbalanced earthquake cycle in Himalayan
581 topography? Geology 38, 987–990.
582 Miller, S.R., Slingerland, R.L., Kirby E., 2007. Characteristics of steady state fluvial
583 topography above fault-bend folds. Journal of Geophysical Research 112, F04004,
584 doi:10.1029/2007JF000772.
585 Mitchell, S.G., Montgomery, D.R., 2006. Influence of a glacial buzzsaw on the height
586 and morphology of the Cascade Range in central Washington State, USA.
587 Quaternary Research 65, 96–107.
588 Ota, Y., Sangawa, A., 1984. Active faults in the eastern foot area of the Suzuka Range,
589 Central Japan. Geographical Review of Japan 57, 237–262 (in Japanese with
590 English abstract).
591 Research Group for Active Faults of Japan, 1991. Active Faults in Japan, Sheet Maps

京都大学 KYOTO UNIVERSITY
A Self-archived copy in
Kyoto University Research Information Repository
https://repository.kulib.kyoto-u.ac.jp
京都大学学術情報リポジトリ KURENAI 紅 Kyoto University Research Information Repository

592 and Inventories (Revised Edition). University of Tokyo Press (in Japanese).
593 Roering, J.J., Kirchner, J.W., Dietrich, W.E., 1999. Evidence for non-linear, diffusive
594 sediment transport on hillslopes and implications for landscape morphology. Water
595 Resources Research 35, 853–870.
596 Sagiya, T., 2004. A decade of GEONET: 1994-2003 -The continuous GPS observation
597 in Japan and its impact on earthquake studies-. Earth, Planets and Space 56, xxix-xli.
598 Schmidt, K.M., Montgomery, D.R., 1995. Limits to Relief. Science 270, 617–620.
599 Seidl, M.A., Dietrich, W.E., 1992. The problem of channel erosion into bedrock.
600 Catena Supplement 23, 101–124.
601 Smith, D.E., Zuber, M.T., Solomon, S.C., Phillips, R.J., Head, J.W., Garvin, J.B.,
602 Banerdt, W.B., Muhleman, D.O., Pettengill, G.H., Neumann, G.A., Lemoine, F.G.,
603 Abshire, J.B., Aharonson, O., Brown, C.D., Hauck, S.A., Ivanov, A.B., McGovern,
604 P.J., Zwally, H.J., Duxbury, T.C., 1999. The global topography of Mars and
605 implications for surface evolution. Science 284, 1495–1503.
606 Stark, C.P., Hovius, N., 2001. The characterization of landslide size distributions.
607 Geophysical Research Letters 28, 1091–1094.
608 Stock, J.D., Montgomery, D.R., 1999. Geologic constraints on bedrock river incision
609 using the stream power law. Journal of Geophysical Research 104, 4983–4994.
610 Tarboton D.G., Bras, R.L., Rodriguez-Iturbe I., 1989. Scaling and elevation in river
611 networks. Water Resources Research 25, 2037–2051.
612 Terakawa, T., Matsu'ura, M., 2010. 3-D tectonic stress fields in and around Japan
613 inverted from CMT data of seismic events. Tectonics 29, TC6008,
614 doi:10.1029/2009TC002626.
615 Thatcher, W., Rundle, J.B., 1984. A viscoelastic coupling model for the cyclic
616 deformation due to periodically repeated earthquakes at subduction zones. Journal of
617 Geophysical Research 89, 7631–7640.
618 Tucker, G.E., Bras, R.L., 2000. A stochastic approach to modeling the role of rainfall
619 variability in drainage basin evolution. Water Resources Research 36, 1953–1964.
620 Tucker, G.E., Slingerland, R.L., 1994. Erosional dynamics, flexural isostasy, and

京都大学 KYOTO UNIVERSITY
A Self-archived copy in
Kyoto University Research Information Repository
https://repository.kulib.kyoto-u.ac.jp
京都大学学術情報リポジトリ KURENAI 紅 Kyoto University Research Information Repository

621 long-lived escarpments: A numerical modeling study. Journal of Geophysical
622 Research 99, 12229–12243.
623 Tucker, G.E., Slingerland, R.L., 1997. Drainage Basin Responses to Climate Change.
624 Water Resources Research 33, 2031–2047.
625 Tucker, G.E., Whipple, K.X., 2002. Topographic outcomes predicted by stream erosion
626 models: Sensitivity analysis and intermodel comparison. Journal of Geophysical
627 Research 107, 2179, doi:10.1029/2001JB000162.
628 Tucker, G.E., Lancaster, S.T., Gasparini, N.M., Bras, R.L. Rybarczyk, S.M., 2001. An
629 Object-Oriented Framework for Hydrologic and Geomorphic Modeling Using
630 Triangulated Irregular Networks. Computers & Geosciences 27, 959–973.
631 van der Beek, P., Bishop, P., 2003. Cenozoic river profile development in the Upper
632 Lachlan catchment (SE Australia) as a test of quantitative fluvial incision models.
633 Journal of Geophysical Research 108, 2309, doi:10.1029/2002JB002125.
634 Wessel, P., Smith, W. H. F., 1998. New, improved version of Generic Mapping Tool
635 released. Eos, Transactions, American Geophysical Union 79, 579.
636 Whipple, K.X., Tucker, G.E., 1999. Dynamics of the stream-power river incision
637 model: Implications for height limits of mountain ranges, landscape response
638 timescales, and research needs. Journal of Geophysical Research 104, 17661–17674.
639 Whipple, K.X., Hancock, G.S., Anderson, R.S., 2000. River incision into bedrock:
640 Mechanics and relative efficacy of plucking, abrasion, and cavitation. Geological
641 Society of America Bulletin 112, 490–503.
642 Willett, S.D., 1999. Orogeny and orography: the effects of erosion on the structure of
643 mountain belts. Journal of Geophysical Research 104, 28957–28981.
644 Willett, S.D., Fisher, D., Fuller, C., Yeh, E.C., Lu, C.Y., 2003. Erosion rates and
645 orogenic wedge kinematics in Taiwan inferred from apatite fission track
646 thermochronometry. Geology 31, 945–948.
647 Willett, S.D., Slingerland, R., Hovius, N., 2001. Uplift, Shortening, and Steady State
648 Topography in Active Mountain Belts. American Journal of Science 301, 455–485.
649 Willgoose, G., Bras, R.L., Rodriguez-Iturbe, I., 1991. A coupled channel network

京都大学 KYOTO UNIVERSITY
A Self-archived copy in
Kyoto University Research Information Repository
https://repository.kulib.kyoto-u.ac.jp
京都大学学術情報リポジトリ KURENAI 紅 Kyoto University Research Information Repository

growth and hillslope evolution model, 1, Theory. Water Resources Research 27, 1671–1684.

Yamano, M., 1995. Recent heat flow studies in and around Japan. In: Gupta M.L., Yamano, M. (Eds.), Terrestrial Heat Flow and Geothermal Energy in Asia. Oxford & IBH Publishing Co., New Dehli, pp. 173–201.

京都大学 KYOTO UNIVERSITY
A Self-archived copy in
Kyoto University Research Information Repository
https://repository.kulib.kyoto-u.ac.jp
京都大学学術情報リポジトリ KURENAI 紅 Kyoto University Research Information Repository

655 **Figure Captions**

656

657 Fig. 1. Profile of asymmetric rock uplift rate in the *x* (east-west) direction, equivalent
658 to Eq. (3). x_u and u_{max} represent the location of the rock uplift axis and the
659 maximum rock uplift rate, respectively. The rock uplift rate is uniform in the *y*
660 (north-south) direction and constant over time.

661 Fig. 2. Topographic evolution process under a given asymmetric rock uplift rate. The
662 initial topography is flat with an elevation of 0 m and superimposed white-noise
663 topography with a maximum amplitude of 10 m. (A) Snapshots of topography over
664 4 My of elapsed time, with a contour interval of 1000 m. (B) East-west topographic
665 profiles averaged in the *y* (north-south) direction. x_t and h_{max} are the location and
666 elevation of the topographic axis in the steady state, respectively. The rock uplift
667 axis x_u, represented by the thick broken line in each diagram, is 30 km, and the
668 maximum uplift rate u_{max} is 6 mm yr^{-1}. Water is drained only from the western
669 (left) and eastern (right) boundaries.

670 Fig. 3. Relation of the location of the topographic axis in the steady state x_t to the
671 maximum rock uplift rate u_{max} for various rock uplift axes x_u. To suppress the
672 effect of the initial random noise, the numerical simulation was performed five times
673 for each pair of u_{max} and x_u. The solid diamond and error bar represent the
674 average and standard deviation of the five trials, respectively.

675 Fig. 4. Relation between parameters of rock uplift and topography. (A) Relation of the
676 height h_{max} at the topographic axis in the steady state to x_u and u_{max}. In order to
677 compare results, the height at the topographic axis is normalized by u_{max}. (B) The
678 relation of the elapsed time to steady state versus x_u and u_{max}. The solid diamond
679 and error bar in each diagram represent the average and standard deviation of the
680 five trials, respectively, for each pair of x_u and u_{max}.

681 Fig. 5. Relation of the location of the topographic axis in the steady state x_t to the
682 location of the rock uplift axis x_u. The numerical results are fitted by a natural
683 logarithmic function in Eq. (5). In this figure, parameter *a* is 22.2 km. The solid

京都大学 KYOTO UNIVERSITY
A Self-archived copy in
Kyoto University Research Information Repository
https://repository.kulib.kyoto-u.ac.jp
京都大学学術情報リポジトリ KURENAI 紅 Kyoto University Research Information Repository

684 diamond and error bar represent the average and standard deviation of 15 trials,
685 respectively. For reference, $x_t = x_u$ is also shown (dotted line).

686 Fig. 6. Relation between x_t and x_u for various pairs of the exponents *m* and *n*. The
687 solid diamond and error bar represent the average and standard deviation of 15 trials,
688 respectively, for the numerical simulation with different random noise of initial
689 topography. The fitted logarithmic function for each pair of exponents has the form
690 of Eq. (5), and the fitting parameter *a* is determined by the least-square method. For
691 reference, $x_t = x_u$ is also shown (dotted line).

692 Fig. 7. Relation of the log-fitting parameter *a* (Eq. 5) with the exponents *m* and *n*. (A)
693 Contour map of parameter *a* on the *m* and *n* coordinate plane. (B) Relation between
694 parameter *a* and a linear function of *m* and *n* on a double logarithmic diagram. The
695 solid line represents the fitting function given in Eq. (6).

696 Fig. 8. Relation of the location of the topographic axis in the steady state x_t to an
697 appropriate indicator of the susceptibility of erosion $n - 5m/4$ for various rock
698 uplift axes x_u.

699 Fig. 9. Topography of the Suzuka Range in central Japan. (A) Location map of the
700 Suzuka Range. The rectangle indicates the region where the elevation data were
701 averaged for the topographic cross-section in Fig. 9B. The area of the Kinki triangle
702 is also shown by dotted lines (Research Group for Active Faults of Japan, 1991).
703 The inset shows the tectonic setting of this area; EUR, NAM, and PHS stand for the
704 Eurasian, North American, and Philippine Sea plates, respectively. (B) Topographic
705 cross-section for the Suzuka Range. The cross-section is calculated from the digital
706 map of Japan (Geographical Survey Institute of Japan, 1997) by averaging the
707 elevation data in the direction parallel to the trend of the range. The horizontal
708 distance and relative elevation are normalized by the width of the range L_R and the
709 difference between the maximum and minimum elevations $h_{max} - h_{min}$, respectively.
710 L_R, h_{max}, and h_{min} are about 20 km, 812 m, and 170 m, respectively.

711 Fig. 10. Crustal deformation pattern caused by reverse fault movement. (A) Vertical
712 cross-section of the assumed fault geometry. The slip rate gradually decreases from

京都大学 KYOTO UNIVERSITY
A Self-archived copy in
Kyoto University Research Information Repository
https://repository.kulib.kyoto-u.ac.jp
京都大学学術情報リポジトリ KURENAI 紅 Kyoto University Research Information Repository

713 3 km at depth to zero at the earth's surface. (B) Uplift rate profile at the earth's
714 surface due to the fault motion (solid line), normalized by the maximum rock uplift
715 rate. Rock uplift pattern in the form of Eq. (3) with $x_u = 32\text{km}$ is also shown
716 (broken line). (C) Horizontal displacement profile at the earth's surface due to the
717 fault motion, normalized by the maximum rock uplift rate.

京都大学
KYOTO UNIVERSITY
A Self-archived copy in
Kyoto University Research Information Repository
https://repository.kulib.kyoto-u.ac.jp
京都大学学術情報リポジトリ
KURENAI 紅
Kyoto University Research Information Repository

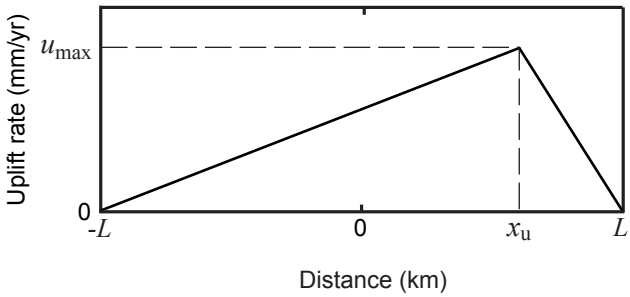

Fig. 1

京都大学 KYOTO UNIVERSITY
A Self-archived copy in
Kyoto University Research Information Repository
https://repository.kulib.kyoto-u.ac.jp
京都大学学術情報リポジトリ KURENAI 紅 Kyoto University Research Information Repository

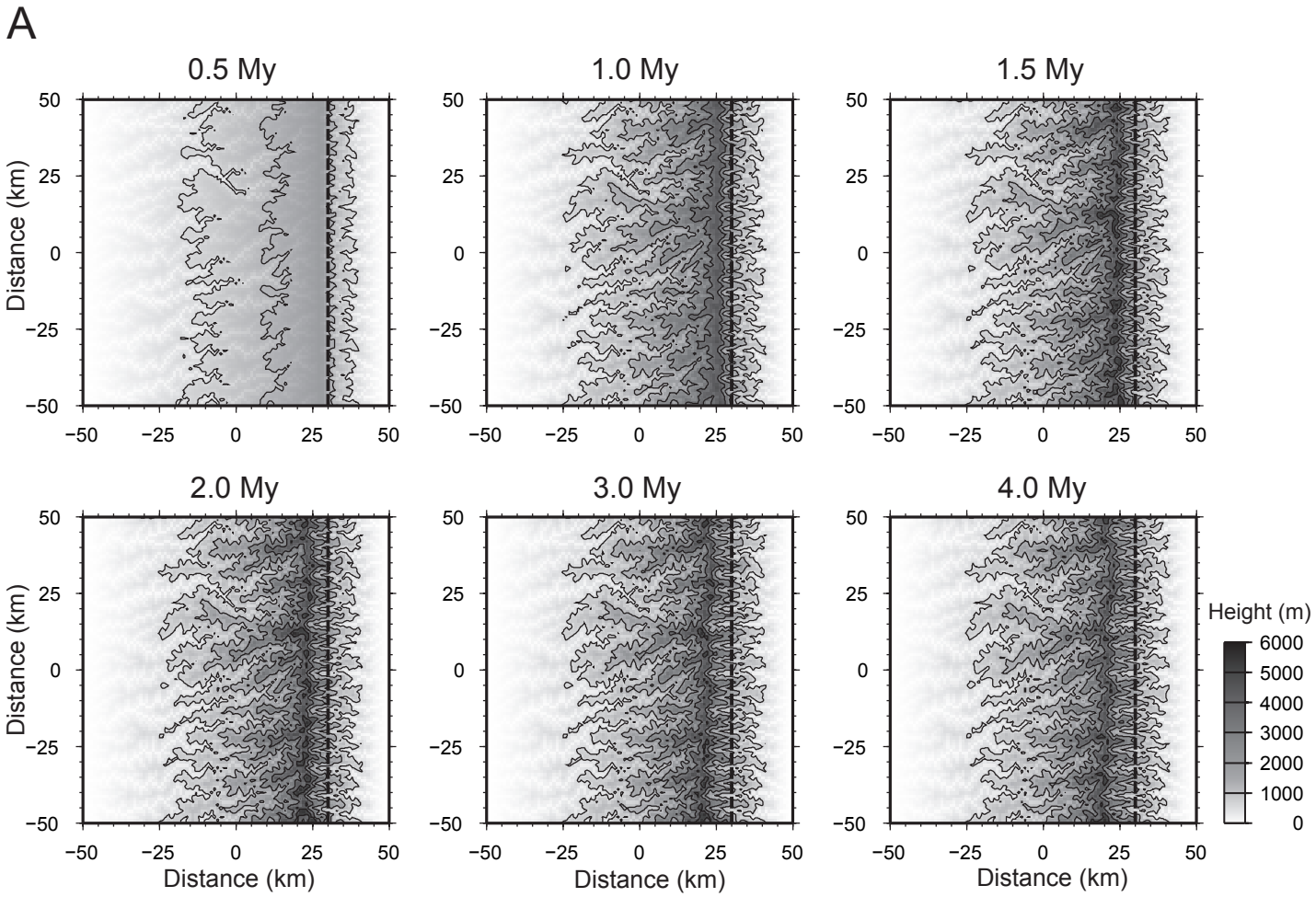

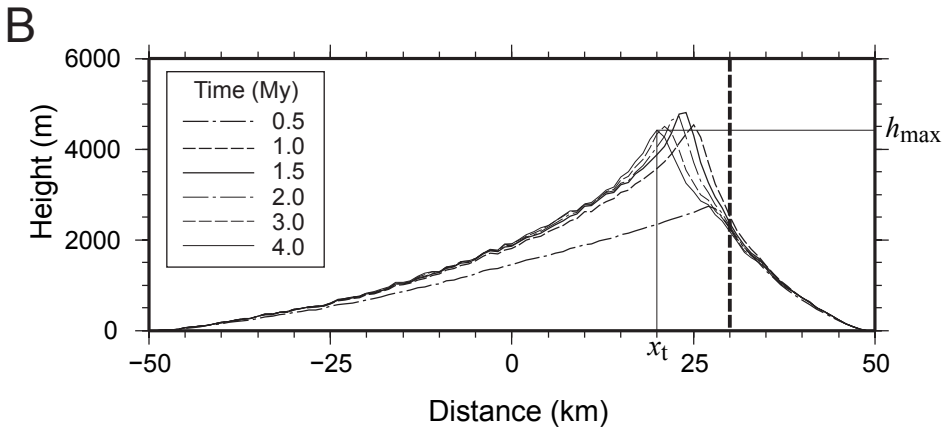

Fig. 2

京都大学 KYOTO UNIVERSITY
A Self-archived copy in
Kyoto University Research Information Repository
https://repository.kulib.kyoto-u.ac.jp
京都大学学術情報リポジトリ KURENAI 紅 Kyoto University Research Information Repository

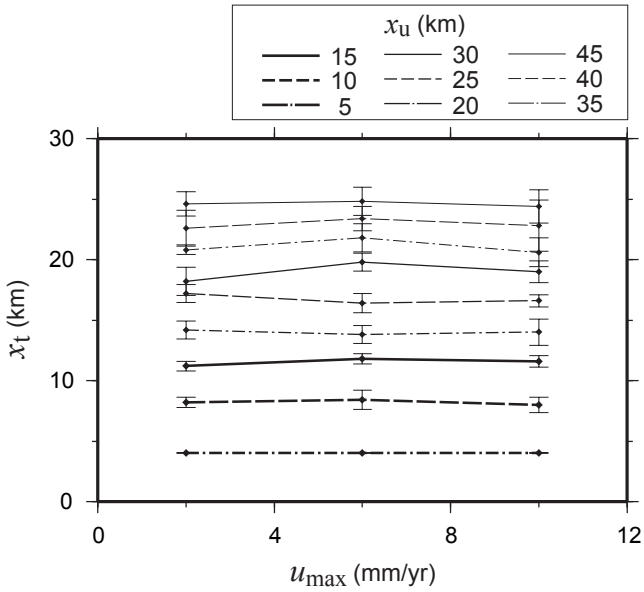

Fig. 3

京都大学 KYOTO UNIVERSITY
A Self-archived copy in
Kyoto University Research Information Repository
https://repository.kulib.kyoto-u.ac.jp
京都大学学術情報リポジトリ KURENAI 紅 Kyoto University Research Information Repository

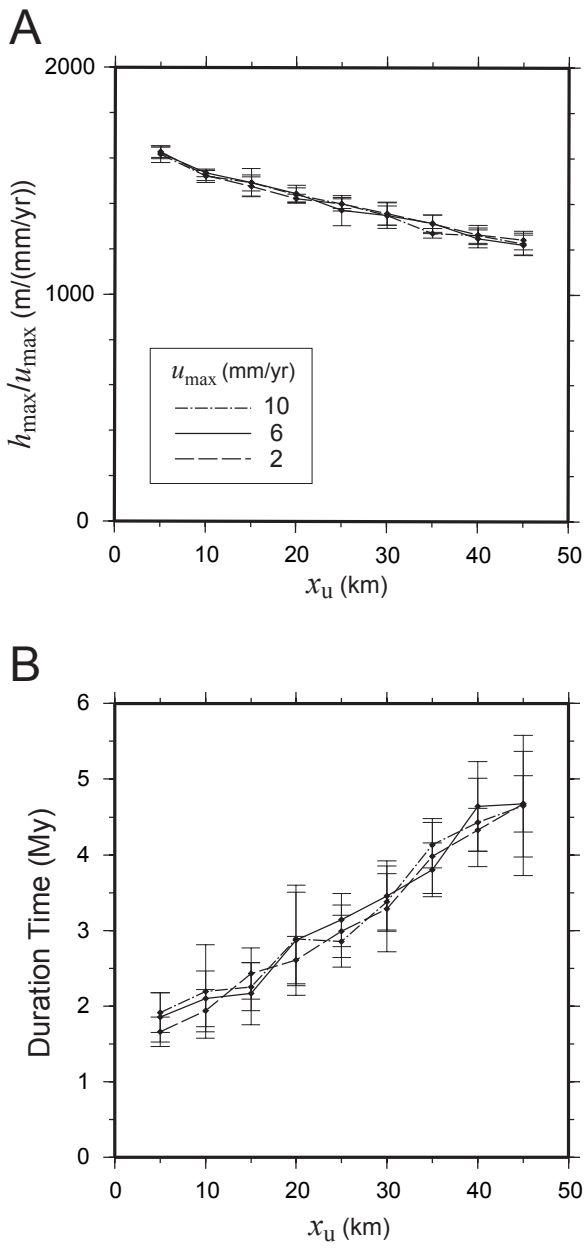

Fig. 4

京都大学
KYOTO UNIVERSITY
A Self-archived copy in
Kyoto University Research Information Repository
https://repository.kulib.kyoto-u.ac.jp
京都大学学術情報リポジトリ
KURENAI 紅
Kyoto University Research Information Repository

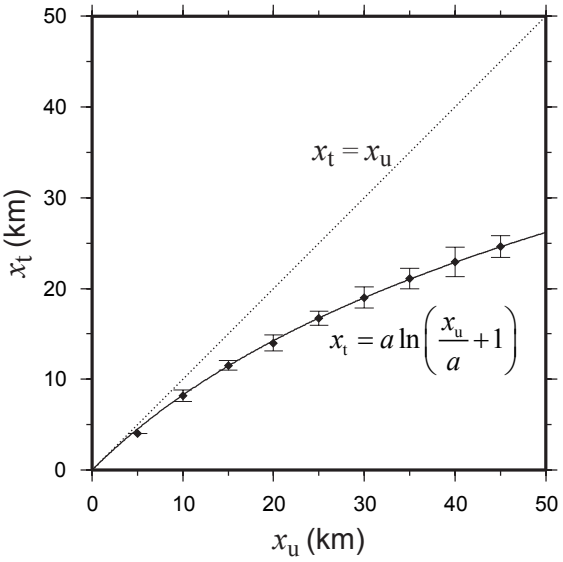

Fig. 5

京都大学 KYOTO UNIVERSITY
A Self-archived copy in
Kyoto University Research Information Repository
https://repository.kulib.kyoto-u.ac.jp
京都大学学術情報リポジトリ KURENAI 紅 Kyoto University Research Information Repository

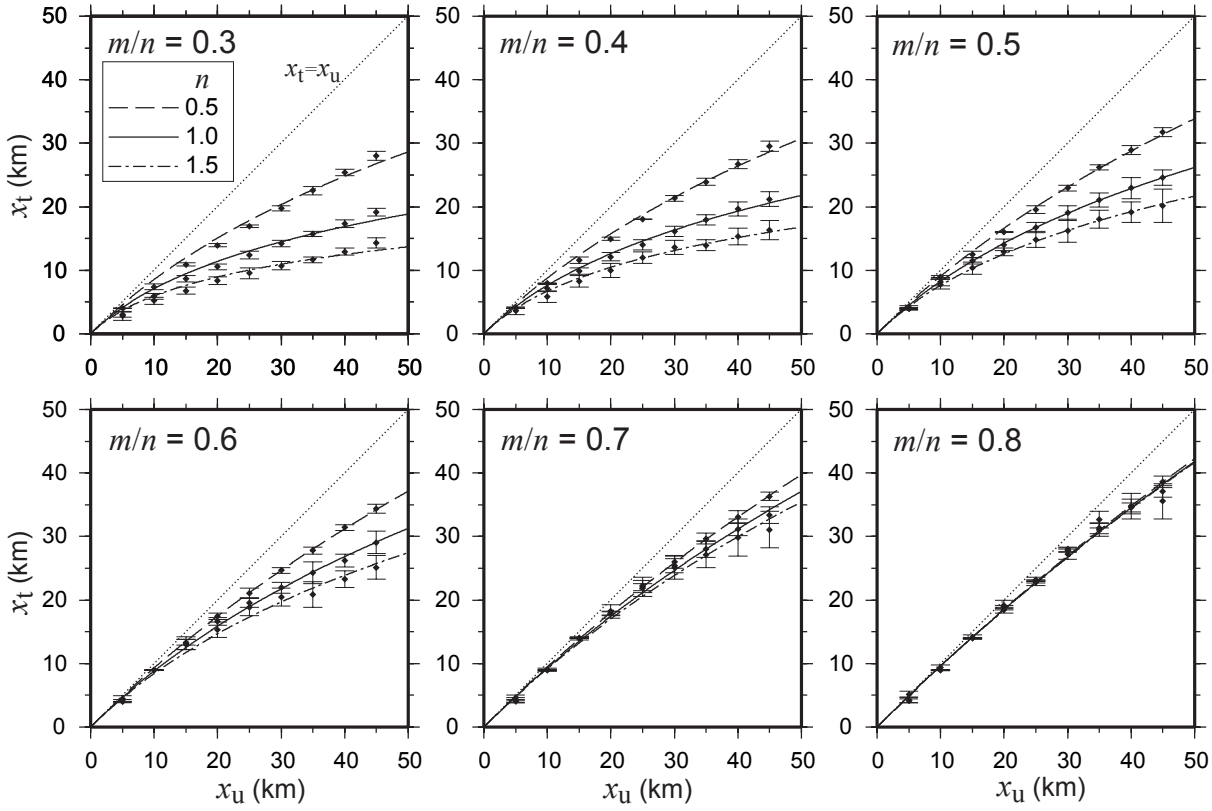

Fig. 6

京都大学 KYOTO UNIVERSITY
A Self-archived copy in
Kyoto University Research Information Repository
https://repository.kulib.kyoto-u.ac.jp
京都大学学術情報リポジトリ KURENAI 紅 Kyoto University Research Information Repository

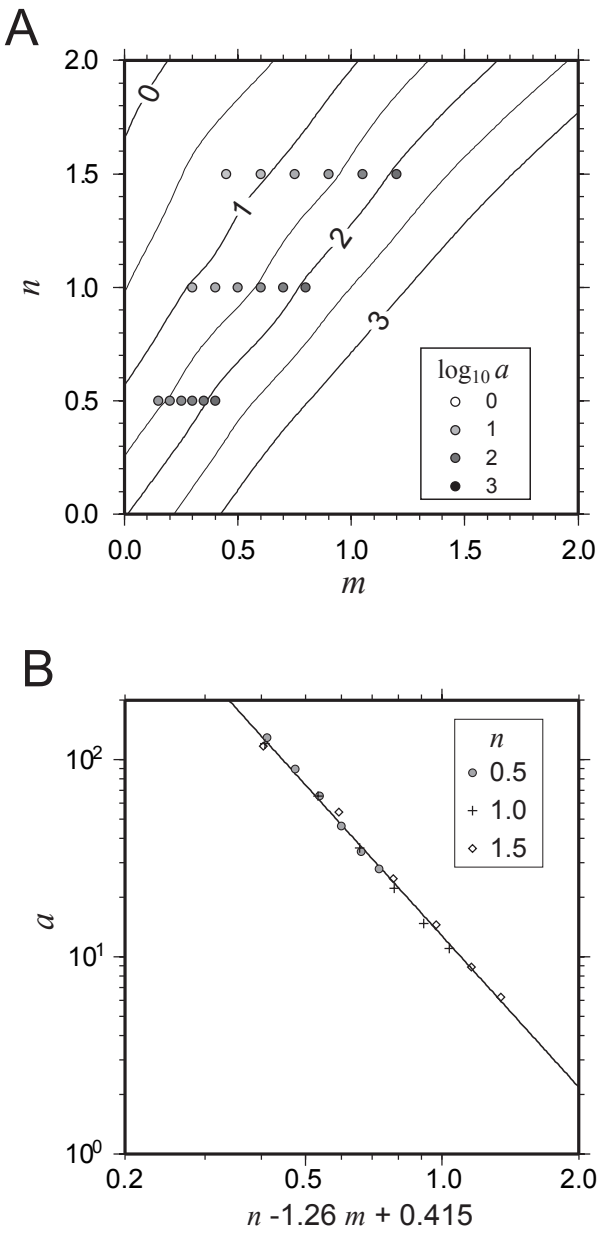

Fig. 7

京都大学
KYOTO UNIVERSITY
A Self-archived copy in
Kyoto University Research Information Repository
https://repository.kulib.kyoto-u.ac.jp
京都大学学術情報リポジトリ
KURENAI 紅
Kyoto University Research Information Repository

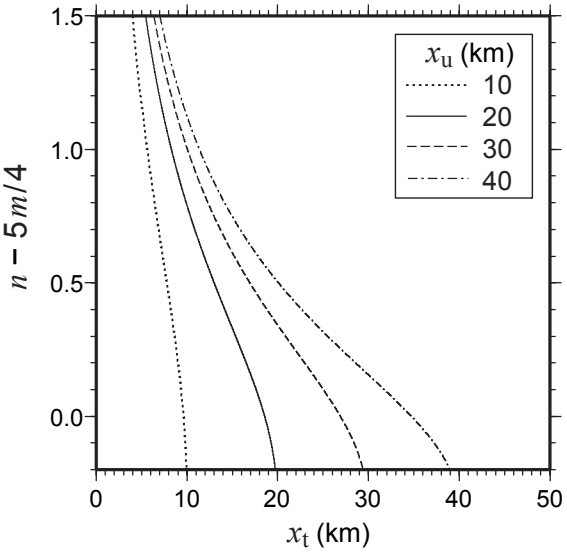

Fig. 8

A Self-archived copy in
Kyoto University Research Information Repository
https://repository.kulib.kyoto-u.ac.jp

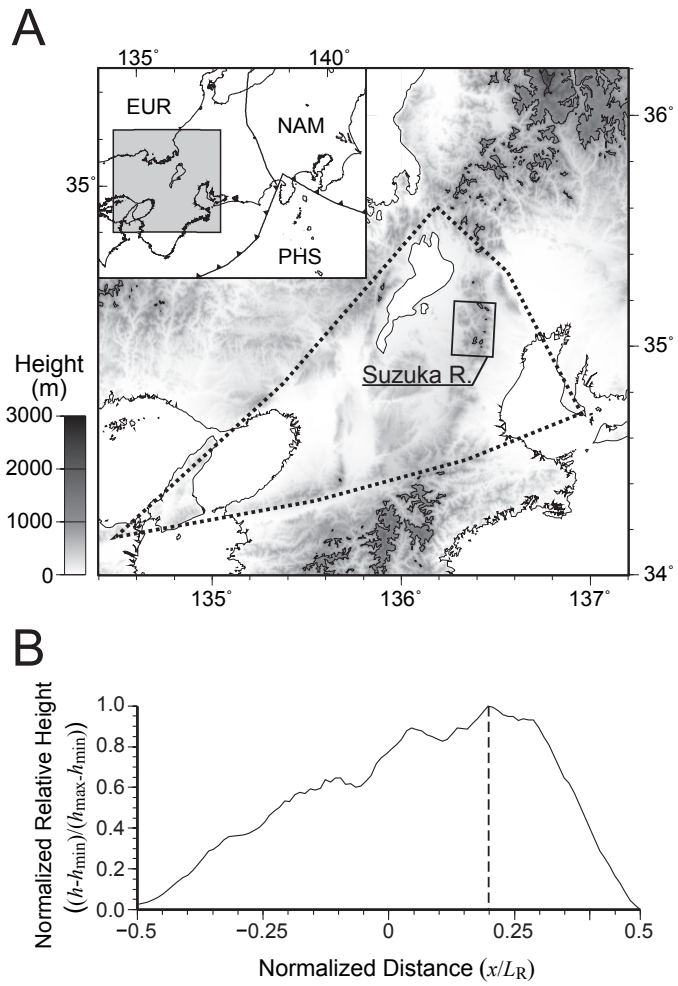

Fig. 9

京都大学
KYOTO UNIVERSITY
A Self-archived copy in
Kyoto University Research Information Repository
https://repository.kulib.kyoto-u.ac.jp
京都大学学術情報リポジトリ
KURENAI 紅
Kyoto University Research Information Repository

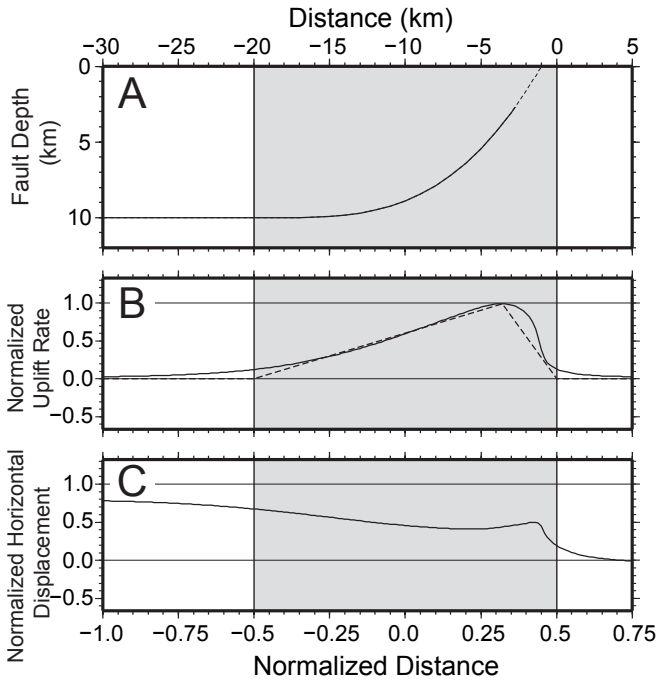

Fig. 10